INSTITUTE OF PHYSICS PUBLISHING JOURNAL OF PHYSICS B: ATOMIC, MOLECULAR AND OPTICAL PHYSICS

J. Phys. B: At. Mol. Opt. Phys. **37** (2004) 3197–3214 PII: S0953-4075(04)81100-3

Photo double ionization spectra of CO: comparison of theory with experiment

John H D Eland[1], Majdi Hochlaf[2], George C King[3], Peter S Kreynin[4], Robert J LeRoy[5], Iain R McNab[4] and Jean-Michel Robbe[6]

[1] Theoretical and Physical Chemistry Laboratory, South Parks Road, Oxford OX1 3QZ, UK
[2] Laboratoire de Chimie Théorique, Université de Marne-La-Vallée, Cité Descartes, 5 Boulevard Descartes, Champs-Sur-Marne, 77454 Marne-La-Vallée Cedex 2, France
[3] Department of Physics and Astronomy, University of Manchester, Manchester, M13 9PL, UK
[4] Department of Physics, School of Natural Sciences, Herschel Building, University of Newcastle upon Tyne, Newcastle upon Tyne NE1 7RU, UK
[5] Department of Chemistry, University of Waterloo, Waterloo, Ontario N2L 3G1, Canada
[6] Laboratoire de Physique des Lasers, Atomes et Molécules, Université de Lille1, Bât. P5, 59655 Villeneuve d'Ascq, France

E-mail: iain.mcnab@ncl.ac.uk

Received 19 May 2004
Published 21 July 2004
Online at stacks.iop.org/JPhysB/37/3197
doi:10.1088/0953-4075/37/15/014

Abstract

High level *ab initio* calculations have been undertaken of potential energy curves of CO^{2+} (and for the CO neutral ground state). The accuracy of the potentials was tested by a synthesis of the available vibrationally resolved threshold photoelectrons in coincidence (TPEsCO) and time of flight, photo electron photo electron coincidence (TOF-PEPECO) spectra of CO^{2+}. Good agreement was found between experimental and theoretical spectra once relative energies of the calculated double ionization energies were slightly adjusted (by approximately 1%) to match experiment. Vibrational separations within individual electronic states are very well reproduced (the worst error is 0.07%).

1. Introduction

Hydrogen is the most abundant molecule in the universe and CO is the second most abundant. Indeed, for the most part estimates of the H_2 content of molecular clouds and galaxies have relied upon determining the abundance of CO (which has electric dipole allowed rotational transitions), and then inferring an H_2 content on the basis of presumed CO/H_2 ratios [1]. The first ion of CO, CO^+ (also written as CO_{II}), occurs in planetary atmospheres, stellar atmospheres, comet tails and in interstellar space [2]. The molecular dication of CO, CO^{2+} (or CO_{III}), is very likely to be present in detectable quantities in some regions of the interstellar

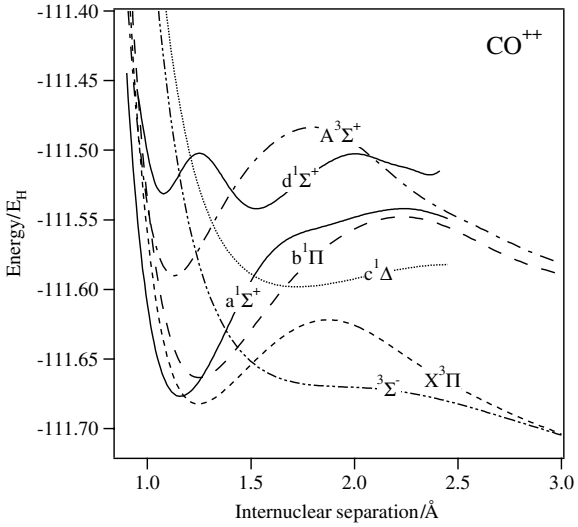

Figure 1. Calculated potential energy curves for the lowest electronic states of CO^{2+} that can contribute to the measurements discussed in this paper.

medium [3], and it is therefore of great interest to determine as many of its spectroscopic and structural properties as possible with a view to guiding future high resolution and astronomical measurements. In this work we have calculated *ab initio* potential energy curves for the lowest electronic states of CO^{2+} at the highest level of theory that is currently achievable, and we compare the theoretical results with the best experimental data that are available to determine their accuracy.

Molecular dications are most easily formed by the double ionization of neutral molecules and are present in some concentration wherever such double ionization processes are possible. However, as for all charged molecules, molecular dications are highly chemically reactive due to long-range interactions (charge/induced-dipole or charge/dipole attraction) with neutral species. For such charged species to be long lived, an environment is therefore required where collision frequencies are low. In addition to the high chemical reactivity, most small molecular dications are also intrinsically thermodynamically unstable. Most electronic states of diatomic molecular dications are purely repulsive due to Coulomb repulsion, but for some states chemical bonding is sufficient to overcome the Coulomb repulsion and create potential wells. Whether such potential wells are thermodynamically stable or not depends upon the ionization potentials for the two atoms concerned [4]. Thermodynamically stable molecular dications were recently reviewed by Schroder and Schwarz [5].

For a generic diatomic dication, AB^{2+}, the identities of the dissociation products are determined by the relative magnitudes of the atomic ionization energies. Provided that the sum of the first two ionization energies of one atom (I_1(A) + I_2(A)) is greater than the sum of the first ionization energies of the two different atoms (I_1(A) + I_1(B)), then the molecule will dissociate to give two charged fragments; this is the case for most light molecular dications. Most electronic states of diatomic dications are therefore purely repulsive due to Coulomb repulsion. However, in some cases chemical bonding interactions are sufficient to overcome the Coulomb repulsion, leading to unusual single- or double-well 'barrier' potential energy curves, examples of which are shown in figure 1. These potentials, each of which has a minimum in an otherwise repulsive potential, have been called 'volcanic potential energy

curves' a term first used to describe similarly shaped potentials arising in alpha-particle decay (see, e.g., [6]). The shapes of the potential energy curves of figure 1 suggest that the barrier may result from an avoided crossing [7], and this appears to be the case for at least the hydrogen halide dications, where analysis of electron densities shows that at short range the molecule may best be considered as $H + X^{2+}$, while at long range it becomes $H^+ + X^+$ (see, e.g., [8]). In contrast, sophisticated calculations for N_2^{2+} and other molecules show that they are usually better thought of as resulting from competition between Coulomb and valence forces [9], as described above.

Each bound potential well has a deep minimum and a high barrier inhibiting dissociation into the charged fragments, and each supports several vibrational levels, all of which are metastable since they lie above the associated dissociation limit. The lower levels can be extremely long lived [17], while the upper levels may dissociate within picoseconds [10]. If population is transferred to such levels, the resulting 'Coulomb explosion' releases considerable kinetic energy (several eV per molecule), which has led to molecular dications being proposed as a source of propulsion [6].

2. The molecular dication CO^{2+}

For CO^{2+} most of the lower electronic states have minima which are capable of supporting vibrational and rotational levels. The levels that are trapped behind the barrier would classically be considered stable, but these levels actually lie in a continuum and can therefore predissociate. All such vibration–rotation states are quasibound and dissociate on timescales which are determined both by the tunnelling rate through the potential barriers, and also by the strength of other predissociation processes such as spin–orbit mediated predissociation (see, e.g., [8]).

There are over forty published papers on the theory, spectroscopy, structure and dynamics of CO^{2+} [11] and it is not our purpose to provide an exhaustive review here. Experiments on CO^{2+} up until 1984 were comprehensively reviewed by Wetmore *et al* [12], and experiments up to 1989 were reviewed by Larsson *et al* [13]. We now briefly review some of the measurements of lifetimes and spectra of CO^{2+} that have been made.

2.1. Lifetimes

The molecular dication CO^{2+} has been of considerable importance in our understanding of the dynamics of dication decay. The spontaneous predissociation of CO^{2+} to C^+ and O^+ on a microsecond timescale was first observed in a mass spectrometer in 1932 [14]. Direct measurement of lifetimes of individual vibrational levels in CO^{2+} has been achieved by two methods. The first measurement relied upon double photoionization using synchrotron radiation. The vibrational levels were determined using pairs of threshold electrons, and the resulting ions characterized by their time of flight. In this manner lifetimes of several states of CO^{2+} were measured and found to have magnitudes of the order of microseconds [15]. The second measurement of vibrational lifetimes used three-dimensional fragment imaging [16] and enabled the simultaneous measurement of kinetic energy release upon dissociation and the lifetime of a given state. Using this technique, lifetimes of two vibrational levels of CO^{2+} were measured as 670 ± 150 ns and 26 ± 5 ns for states with kinetic energy releases of 5.713 eV (assigned as $^1\Pi$, $v = 0$)) and 5.841 eV (assigned as $^1\Sigma^+$, $v = 0$ or 1) respectively. The lifetimes of CO^{2+} levels have also been measured directly in an ion storage ring, providing the first direct evidence that a doubly charged molecule could be stable on a timescale of seconds [17].

Despite these vibrationally resolved studies of lifetimes, the dynamics of the predissociation of CO^{2+} have not yet been fully determined and must await further observations such as high resolution spectra where rotationally resolved lifetimes can be obtained directly from predissociation linewidths [4]. In this work, we calculated lifetimes due to tunnelling predissociation alone (see below).

2.2. Vibrationally resolved spectra

The first coincidence technique to yield vibrationally resolved spectra of molecular dications was the threshold photoelectrons in coincidence (TPEsCO) technique, of King and co-workers [18]. The TPEsCO technique exploits the fact that near zero kinetic energy electrons can be selectively detected with a resolution $\approx$10 meV (81 cm^{-1}), and has been used to great effect to measure vibrationally resolved spectra of many molecular dications, including CO^{2+} (the spectrum of which is reproduced in this paper) and most recently HI^{2+} [19]. The recently developed time-of-flight photoelectron–photoelectron coincidence (TOF-PEPECO) technique uses a pulsed lamp and long magnetic bottle to acquire complete two-electron spectra; it has been applied to many small molecules including CO [36].

Vibrationally resolved spectra of CO^{2+} have also measured by Lundqvist *et al* at Uppsala University [20]. Their instrument produced CO^{2+} by pulsed electron impact on neutral CO gas. Fragment ions due to predissociation of the molecular dications were collected in coincidence at opposite ends of two 50 cm long flight tubes and detected using microchannel plates. By measuring the energies of both fragments, the centre-of-mass kinetic energy was eliminated by a simple calculation (done in real time for each pair of fragments), resulting in a Doppler-free spectrum with vibrational resolution. A vibrationally resolved spectrum of CO^{2+} has also been obtained using double charge transfer spectroscopy by Furuhashi *et al* [21]. The principal difference between the techniques of Lundquist *et al* [20] and Furuhashi *et al* [21] is that Lundquist's spectrum shows dissociative states of both multiplicities, whereas Furuhashi's shows singlets only, whether they are dissociative or not.

2.3. Rotationally resolved electronic spectroscopy

There have been reports of possible rotationally resolved fluorescence of CO^{2+} at 546.3 nm [22]. However in a more recent paper [23] the assignment of this band was questioned, and it was shown that this band probably does not belong to CO^{2+}. In addition, this band could not be rotationally analysed because of overlapping with the lines of $d^3\Delta$–$a^3\Pi$ states of CO. It is also suggested in [23] that the possible fluorescence of CO^{2+} should be limited to six emission lines in the $A^3\Sigma^+$–$X^3\Pi$ transition. There have also been attempts to obtain rotationally resolved spectra of CO^{2+} using ion-beam/laser-beam spectroscopy, which we now discuss.

Following their successful detection of an ion-beam spectrum of N_2^{2+} [24] a substantial but unsuccessful search for a visible spectrum of CO^{2+} was undertaken by Professor P J Sarre and his co-workers [25] using an ion-beam/laser-beam experiment. The two CO^{2+} transitions $A^3\Sigma^+$ ($v = 0$)–$X^3\Pi$ ($v = 0$) (using R110 laser dye which allows scans from 18 273 to 18 433 cm^{-1} with a gap between 18 288 and 18 318 cm^{-1}) and $A^3\Sigma^+$ ($v = 0$)–$X^3\Pi$ ($v = 1$) (using R6G laser dye) were sought but not found. Following their work on N_2^{2+} [26, 27] and NO^{2+} [28, 29] also using an ion-beam/laser-beam experiment, Professor M Larsson and his co-workers also performed an unsuccessful search for an ion-beam spectrum of CO^{2+}, again attempting to pump from the $X^3\Pi$ state to the $A^3\Sigma^+$ state [30].

Table 1. X $^3\Pi$ and A $^3\Sigma^+$ and a repulsive $^3\Sigma^-$ state potential energy curves of CO^{2+} (all energies in Hartree).

Internuclear distance (Å)	$X^3\Pi$ state energy, E_H (CO^{++} ground state)	$A^3\Sigma^+$ state energy (E_H)	$^3\Sigma^-$ state energy (E_H)
0.85	−111.176 203	−111.240 106	−110.813 847
0.90	−111.351 973	−111.384 121	−111.032 418
0.95	−111.475 039	−111.479 334	−111.195 426
1.00	−111.559 302	−111.538 865	−111.317 132
1.05	−111.615 111	−111.572 503	−111.408 099
1.10	−111.650 211	−111.587 606	−111.476 171
1.15	−111.670 425	−111.589 763	−111.527 181
1.20	−111.680 139	−111.583 288	−111.565 467
1.30	−111.680 437	−111.557 449	−111.615 945
1.40	−111.668 600	−111.530 251	−111.644 709
1.50	−111.653 815	−111.510 490	−111.661 218
1.60	−111.640 346	−111.496 744	−111.670 524
1.70	−111.629 895	−111.487 352	−111.675 462
1.80	−111.623 317	−111.482 868	−111.677 866
1.90	−111.621 680	−111.485 328	−111.679 019
2.00	−111.625 686	−111.495 861	−111.679 814
2.20	−111.643 431	−111.520 246	−111.682 759
2.40	−111.662 186	−111.539 901	−111.688 330
2.60	−111.678 370	−111.555 969	−111.696 315
2.80	−111.692 177	−111.569 538	−111.705 194
3.00	−111.704 143	−111.581 312	−111.714 100
3.20	−111.714 670	−111.591 707	−111.722 615
3.40	−111.724 030	−111.600 979	−111.730 569
3.60	−111.732 412	−111.609 306	−111.737 920
3.80	−111.739 964	−111.616 821	−111.744 684
4.00	−111.746 800	−111.623 632	−111.750 899
4.20	−111.753 011	−111.629 826	−111.756 612
4.40	−111.758 677	−111.635 480	−111.761 871
4.60	−111.763 865	−111.640 658	−111.766 722
4.80	−111.768 630	−111.645 416	−111.771 205

3. Theoretical potentials

Potential energy curves for molecular dications are notoriously difficult to calculate to spectroscopic accuracy. For CO^{2+} the first comprehensive set of potentials were calculated by Wetmore *et al* [12], but although these calculations represented the state of the art in 1984, by present standards they are of relatively low quality. Prior to the present work, the most accurate potentials available were those of Larsson and his co-workers [13, 17]. Our potentials were calculated with a larger basis set than Larsson's and included a full valence MRCI treatment.

A full tabulation of the calculated potentials (including that for the CO neutral ground electronic state) is given in tables 1–5; the number of digits given yields smooth potentials for interpolation, and is not intended to indicate the absolute accuracy of the calculation. Figure 1 shows the short bond length part of the resulting calculated potentials. The absolute accuracy of the calculation can best be found by the comparison with experiment that we give below.

Table 2. $a^1\Sigma^+$ and $d^1\Sigma^+$ state potential energy curves of CO^{2+} (all energies in Hartree).

Internuclear distance (Å)	$a^1\Sigma^+$ state energy (E_H)	$d^1\Sigma^+$ state energy (E_H)
0.900	−111.444 483	−111.372 22
0.950	−111.545 137	−111.455 69
1.000	−111.610 540	−111.503 13
1.050	−111.649 674	−111.524 83
1.100	−111.669 941	−111.528 73
1.125	−111.674 764	−111.525 95
1.150	−111.676 807	−111.520 92
1.175	−111.676 547	−111.514 37
1.200	−111.674 397	−111.507 20
1.225	−111.670 716	−111.500 91
1.250	−111.665 812	−111.498 16
1.275	−111.659 956	−111.500 75
1.300	−111.653 384	−111.506 52
1.325	−111.646 300	−111.512 82
1.350	−111.638 878	−111.518 69
1.375	−111.631 268	−111.523 87
1.400	−111.623 599	−111.528 31
1.450	−111.608 532	−111.535 06
1.500	−111.594 498	−111.539 13
1.550	−111.582 300	−111.540 50
1.600	−111.572 792	−111.538 94
1.650	−111.566 387	−111.534 46
1.700	−111.562 354	−111.528 13
1.750	−111.559 477	−111.521 39
1.800	−111.557 011	−111.515 20
1.850	−111.554 656	−111.510 02
1.900	−111.552 608	−111.506 50
1.950	−111.550 351	−111.504 07
1.975	−111.549 256	−111.503 41
2.000	−111.548 195	−111.503 12
2.025	−111.547 176	−111.503 23
2.050	−111.546 205	−111.503 67
2.075	−111.545 295	−111.504 43
2.100	−111.544 457	−111.505 47
2.125	−111.543 707	−111.506 70
2.150	−111.543 066	−111.508 05
2.175	−111.542 557	−111.509 46
2.200	−111.542 201	−111.510 86
2.250	−111.542 046	−111.513 43
2.300	−111.542 733	−111.515 42
2.350	−111.544 245	−111.516 61
2.400	−111.546 438	−111.516 63
2.450	−111.549 099	−111.513 55

3.1. CI calculations of the potential energy functions

The electronic structure computations were performed with state-averaged full valence complete active space self-consistent field (CASSCF) [31] and internally contracted multireference configuration interaction (MRCI) approaches [32].

For mapping the CASSCF potential energy functions (PEFs), an spdf cc-pV5Z basis set [33] was used for C and O, which resulted in 160 contracted Gaussian functions. The $X^3\Pi$

Table 3. $b^1\Pi$ state potential energy curve of CO^{2+} (all energies in Hartree).

Internuclear distance (Å)	$b^1\Pi$ state energy (E_H)	Internuclear distance (Å)	$b^1\Pi$ state energy (E_H)
0.900	−111.323 964	1.850	−111.571 053
0.950	−111.448 947	1.900	−111.565 357
1.000	−111.534 968	1.950	−111.560 440
1.050	−111.592 354	1.975	−111.558 283
1.100	−111.628 816	2.000	−111.556 338
1.125	−111.641 069	2.025	−111.554 609
1.150	−111.650 136	2.050	−111.553 094
1.175	−111.656 516	2.075	−111.551 798
1.200	−111.660 642	2.100	−111.550 723
1.225	−111.662 886	2.125	−111.549 860
1.250	−111.663 570	2.150	−111.549 203
1.275	−111.662 968	2.175	−111.548 745
1.300	−111.661 318	2.200	−111.548 465
1.325	−111.658 822	2.250	−111.548 454
1.350	−111.655 651	2.300	−111.549 437
1.375	−111.651 952	2.350	−111.550 502
1.400	−111.647 850	2.400	−111.551 355
1.450	−111.638 839	2.450	−111.553 604
1.500	−111.629 272	2.600	−111.567 928
1.550	−111.619 597	2.700	−111.573 709
1.600	−111.610 122	2.800	−111.579 276
1.650	−111.601 057	3.000	−111.589 545
1.700	−111.592 542	3.250	−111.600 880
1.750	−111.584 671	3.500	−111.610 832
1.800	−111.577 497	4.000	−111.623 826

and the $A^3\Sigma^+$ wavefunctions were simultaneously averaged at all internuclear separations in the C_{2v} symmetry, with 592 configurational state functions (CSFs) in the $X^3\Pi$ and 584 CSFs in the $A^3\Sigma^+$. This procedure is necessary to calculate transition moment functions between states belonging to different symmetries. All CSFs from the CASSCF approach were taken as reference in the MRCI calculations in which all valence electrons were correlated. In the MRCI calculations each symmetry species was calculated separately. The electronic structure computations were done with the Molpro program suite [34].

Calculations were made for seven electronic states: the three lowest triplets $X^3\Pi$, $A^3\Sigma^+$ and a repulsive $^3\Sigma^-$ state, and the four lowest singlet states: $b^1\Pi$, $a^1\Sigma^+$, $d^1\Sigma^+$ and $c^1\Delta$. It was relatively simple to calculate the potentials for these triplets states, since each one is the lowest state with that symmetry, but the problem was a little more challenging for the singlet states. At large internuclear separation, repulsive states appear in the CI diagonalization and perturb the ordering of states. Increasing the number of states in the diagonalization introduced convergence problems for distances beyond 2.45 Å for the $^1\Sigma^+$ and $^1\Delta$ states. This problem has also been noted by others; see for example [13].

3.2. Calculations of tunnelling linewidths (lifetimes)

In this work we calculated the tunnelling widths of vibrational levels supported by each potential; we report the calculated widths for all states except the $c^1\Delta$ and $d^1\Sigma^+$ states. Each potential was extrapolated to long bond length using an assumed C_1/R functional form,

Table 4. $c^1\Delta$ state potential energy curve of CO^{2+} (all energies in Hartree).

Internuclear distance (Å)	$c^1\Delta$ state energy (E_H)	Internuclear distance (Å)	$c^1\Delta$ state energy (E_H)
1.000	−111.253 44	1.750	−111.598 43
1.050	−111.343 63	1.800	−111.597 06
1.100	−111.410 84	1.850	−111.596 70
1.125	−111.439 56	1.900	−111.595 65
1.150	−111.460 96	1.950	−111.594 10
1.175	−111.482 56	1.975	−111.593 29
1.200	−111.498 34	2.000	−111.592 46
1.225	−111.514 61	2.025	−111.591 62
1.250	−111.527 44	2.050	−111.590 79
1.275	−111.538 51	2.075	−111.589 96
1.300	−111.546 99	2.100	−111.589 15
1.325	−111.556 31	2.125	−111.588 36
1.350	−111.563 41	2.150	−111.587 59
1.375	−111.569 52	2.175	−111.586 85
1.400	−111.573 91	2.200	−111.586 15
1.450	−111.583 16	2.250	−111.584 88
1.500	−111.588 45	2.300	−111.583 84
1.550	−111.593 46	2.350	−111.583 02
1.600	−111.595 50	2.400	−111.582 45
1.650	−111.597 84	2.450	−111.582 13
1.700	−111.597 79		

Table 5. $X^1\Sigma^+$ ground-state potential energy curve of neutral CO (all energies in Hartree).

Internuclear distance (Å)	CO $X^1\Sigma^+$ energy (E_H)
1.00	−113.141 108
1.05	−113.175 716
1.10	−113.191 218
1.15	−113.193 084
1.20	−113.185 384
1.30	−113.152 602
1.40	−113.108 804
1.50	−113.062 541
1.60	−113.018 188
1.70	−112.977 794
1.80	−112.942 146
1.90	−112.911 383
2.00	−112.885 330
2.20	−112.845 948
2.40	−112.820 608
2.80	−112.791 251
3.00	−112.788 977

together with an asymptotic dissociation energy. The asymptotic dissociation energies were calculated from the last calculated point of each potential, at longest bond length, by assuming that this was a pure Coulomb energy between two point charges. In fact, providing that the asymptotic energy is below the potential minimum, the calculations of tunnelling width are

Table 6. Tunnelling widths (in cm^{-1}) for the vibrational levels of the potentials investigated; no tunnelling linewidths are reported for the $c^1\Delta$ and $d^1\Sigma^+$ potentials because insufficient long bond length information was calculated to enable an accurate asymptotic extrapolation of the potentials. These widths represent a lower limit, as the states are also affected by spin–orbit mediated predissociation and radiative decay (the widths in cm^{-1} may be converted to lifetimes in seconds using the formula $\tau(s) = 1/2\pi c(\text{cm s}^{-1})\,\Gamma(\text{cm}^{-1}) = 1/1.883\,65 \times 10^{11}\Gamma(\text{cm}^{-1})$). The symbol '‡' indicates widths less than the numerical precision of the calculations.

V	$X^3\Pi$	$A^3\Sigma^+$	$a^1\Sigma^+$	$b^1\Pi$
0	$0.416\,69 \times 10^{-55}$	‡	‡	‡
1	$0.561\,33 \times 10^{-47}$	‡	‡	‡
2	$0.879\,33 \times 10^{-40}$	‡	‡	‡
3	$0.266\,41 \times 10^{-33}$	$0.245\,43 \times 10^{-65}$	‡	‡
4	$0.193\,99 \times 10^{-27}$	$0.130\,12 \times 10^{-55}$	‡	‡
5	$0.405\,54 \times 10^{-22}$	$0.601\,52 \times 10^{-47}$	‡	‡
6	$0.270\,57 \times 10^{-17}$	$0.322\,42 \times 10^{-39}$	‡	‡
7	$0.634\,67 \times 10^{-13}$	$0.244\,73 \times 10^{-32}$	‡	‡
8	$0.576\,99 \times 10^{-09}$	$0.309\,79 \times 10^{-26}$	‡	‡
9	$0.211\,82 \times 10^{-05}$	$0.793\,48 \times 10^{-21}$	‡	‡
10	$0.307\,59 \times 10^{-02}$	$0.508\,88 \times 10^{-16}$	‡	$0.411\,00 \times 10^{-65}$
11	1.4970	$0.950\,88 \times 10^{-12}$	$0.256\,33 \times 10^{-64}$	$0.125\,08 \times 10^{-56}$
12		$0.575\,19 \times 10^{-08}$	$0.424\,19 \times 10^{-54}$	$0.701\,06 \times 10^{-49}$
13		$0.122\,46 \times 10^{-04}$	$0.109\,25 \times 10^{-44}$	$0.804\,88 \times 10^{-42}$
14		$0.100\,27 \times 10^{-01}$	$0.426\,41 \times 10^{-36}$	$0.203\,21 \times 10^{-35}$
15		2.9300	$0.190\,44 \times 10^{-28}$	$0.132\,40 \times 10^{-29}$
16			$0.542\,49 \times 10^{-22}$	$0.286\,96 \times 10^{-24}$
17			$0.860\,13 \times 10^{-17}$	$0.135\,72 \times 10^{-19}$
18			$0.185\,85 \times 10^{-12}$	$0.156\,78 \times 10^{-15}$
19			$0.909\,32 \times 10^{-09}$	$0.887\,08 \times 10^{-12}$
20			$0.136\,73 \times 10^{-05}$	$0.314\,46 \times 10^{-08}$
21			$0.931\,76 \times 10^{-03}$	$0.807\,56 \times 10^{-05}$
22			0.254 07	$0.188\,75 \times 10^{-01}$
23			20.115	11.488

very insensitive to the energy asymptote used, or to the functional form of the extrapolation providing it approaches the asymptote smoothly from above. However, even using this approach, insufficient long bond length information was calculated to enable an accurate asymptotic extrapolation of the $c^1\Delta$ and $d^1\Sigma^+$ potentials, and so no tunnelling predissociation linewidths are reported for these states. However, this extrapolation was used for the forward calculation of the spectra reported below, including the $c^1\Delta$ and $d^1\Sigma^+$ states. Fortunately the experimental spectral linewidths are determined (for the classically bound states) not by the natural widths of the levels involved, but by the energy resolution of the experiments which is typically around 100 meV. Note too that ambiguity regarding details of this extrapolation will have no significant effect on the broad high energy c-state 'reflection' spectrum discussed below.

Those tunnelling widths that were calculated, presented in table 6, represent lower limits to the real widths (equivalently, an upper limit to real lifetimes) that will also be affected by spin–orbit mediated predissociation. We reserve for future work a full calculation of lifetimes based on the potentials presented here, together with couplings between them, and the effect of lifetimes on possible measurements of high resolution spectra and possible observations of CO^{2+} in the interstellar medium [35].

Table 7. Theoretically determined spectroscopic constants of the electronic ground state of CO and the lowest electronic states of CO^{2+}. All values are in cm^{-1} unless otherwise specified.

	CO	CO^{2+}					
	$X^1\Sigma^+$	$X^3\Pi$	$a^1\Sigma^+$	$A^3\Sigma^+$	$b^1\Pi$	$c^1\Delta$	$d^1\Sigma^{+a,b}$
ω_e	2161.0	1435.2	1920.5	2043.8	1487.7	545.9	1125.6
$\omega_e x_e$	11.90	24.6	16.7	16.3	17.2	38.9	7.59
$\omega_e y_e$	1.84	0.15	0.37	2.49	0.00	6.25	1.55
B_e	1.917	1.579	1.829	1.909	1.573	0.843	1.023
α_e	0.020	0.028	0.021	0.022	0.023	0.048	−0.012
R_e(bohr)	2.1399	2.3581	2.1906	2.1444	2.3621	3.2269	2.9285

[a] The inner potential well supports three vibrational levels located at 1169.4, 3420.9 and 5552.0 (cm^{-1}) relative to the energy of this minimum at $R_e = 2.0427$ bohr. The rotational constants of the inner potential well are $B_e = 2.104\ cm^{-1}$ and $\alpha_e = 0.099\ cm^{-1}$.
[b] Spectroscopic constants for the outer potential well.

4. Simulated spectra and TPEsCO measurements

In order to determine the accuracy of our potentials, we now compare them with the best available experimental data for CO^{2+}, the previously published vibrationally resolved TPEsCO [48, 49] and TOF-PEPECO [36] measurements. Although the TPEsCO measurements are vibrationally resolved, the observed vibrational progressions are short. In these circumstances it is best to examine the accuracy of calculations by performing a direct forward calculation, that is a simulation of the spectra, rather than reducing the spectra to a set of constants and then calculating the values of the constants. Some of us have previously used this approach elsewhere to simulate TPEsCO spectra of HCl^{2+} [38], DCl^{2+} [41], NO^{2+} [37] and HI^{2+} [19]. Spectroscopic constants determined from our *ab initio* potentials are listed in table 7.

4.1. Forward calculations of spectra

Our calculations considered all electronic states of CO^{2+} lying within the energy window of the available experimental data. Since ionization is not believed to cause rotational excitation, the rotational population distribution was assumed to be the Boltzmann distribution for the CO neutral precursor at the ambient temperature of the experiments. We considered rotational states up to $J = 13$, which included at least 99% of the population of the neutral CO. This approach can give only relative intensities of vibrational progressions within a given electronic transition, and takes no account at all of the transition dipole. We allow for the transition dipole empirically, by scaling the calculated electronic bands to match the observed intensities.

In order to simulate spectra from the calculated potentials, we calculated frequencies and Franck–Condon factors for photo double ionization from the neutral ground state of CO in a 'Q-branch' approximation (see [38] and references therein) using the two programs BCONT[7] [39] and LEVEL[7] [40]. The validity of our approach to calculating photo double ionization spectra has been discussed in detail elsewhere in connection with the TPEsCO spectra of the molecular dications HCl^{2+} and DCl^{2+} [37, 41]. In that work it was shown that the experimental vibrational spectra include continuum resonances that are supported by the potential, but which lie above the barrier maximum. For a complete calculation of the vibrational structure of a molecular dication one should therefore consider not only levels that lie below the barrier maximum, but also those continuum resonances that lie above the barrier

[7] See the 'Computer Programs' link at http://leroy.uwaterloo.ca.

maximum [38, 41]. The widths of such resonances increase rapidly with the energy above the barrier maximum [42], and it is not clear that they have been observed in the spectra of CO^{2+}. Strictly speaking, all vibration–rotation structures of dications with 'volcanic' potential energy curves are resonance states lying in the continuum, and should therefore be evaluated in a scattering treatment. BCONT is a program that is able to evaluate transition intensities to the final states that lie in the continuum, and enables us to make calculations to states that are above the barrier. The continuum eigenfunctions are generated using the Numerov algorithm [43].

Although they do lie in the continuum, vibration–rotation levels which lie far below the potential energy maxima have extremely narrow linewidths, and BCONT cannot reliably locate the narrowest resonances using only standard double precision arithmetic. To address this problem we used the bound-state program LEVEL which can automatically locate and calculate the widths of tunnelling predissociation levels lying below a barrier maximum. LEVEL uses the Numerov–Cooley [43, 44] algorithm with a special boundary condition to solve the radial Schrödinger equation for quasibound levels. In order to ensure that the two calculations were accurately connected to one another, we always treated at least one intermediate-width resonance level by both methods. The Franck–Condon factor for the transition calculated by LEVEL was normalized to the area under the peak calculated with BCONT, and this normalization factor was then applied to all levels calculated using LEVEL.

Finally, a simulated spectrum was produced by convoluting the calculated peak positions and intensities with a Gaussian function designed to mimic the experimentally observed linewidths (we used a FWHM of 650 cm^{-1}). Generally the convolution process is described by the integral:

$$z(t) = x(t) * y(t) = \int_{-\infty}^{+\infty} x(\tau)y(t-\tau)\,\mathrm{d}\tau,$$

(see, e.g., [45]). In our case $x(\tau)$ is the calculated spectrum and $y(t-\tau)$ is a Gaussian function defined on the same grid of energy points as the simulated spectra. This convolution was performed using a separate (FORTRAN) program [46], a key feature of which is an adaptive step length algorithm that enables us to work with arrays that do not have a constant energy mesh. Such non-uniformity was required when we used BCONT with smaller energy increments to calculate some transitions and amplitudes to the desired accuracy.

Our calculations for CO^{2+} yielded the predicted resonance structure above the barrier maxima for some states, but these were in general too broad, and hence too weak to have been observed experimentally. However, in the case of the $X^3\Pi$ state, the above-barrier resonances are predicted to have intensities greater than those of resonances that correspond to the last classically bound levels, as shown in figure 2. Careful inspection of the measured data does not provide any evidence that these above-barrier resonances contribute to the structure in the low-energy part of the spectrum, but given the complexity of the spectrum in this region we cannot be sure that the above-resonance levels do not contribute to the measured spectra.

Franck–Condon Factors give the relative intensities for transitions into the different vibrational levels of a particular electronic state of CO^{2+}. It has often been found that the measured intensities in TPEsCO spectra are due to indirect double ionization processes, and hence are not well reproduced by a Franck–Condon calculation using a constant transition moment function. Happily, for the CO^{2+} spectra reconsidered in this paper, Franck–Condon intensities appear to reproduce quite satisfactorily the measured relative intensities within a particular electronic state. We can therefore infer that indirect double ionization processes do not make a large contribution to the double ionization spectra of CO recorded by the TPEsCO or TOF-PEPECO techniques.

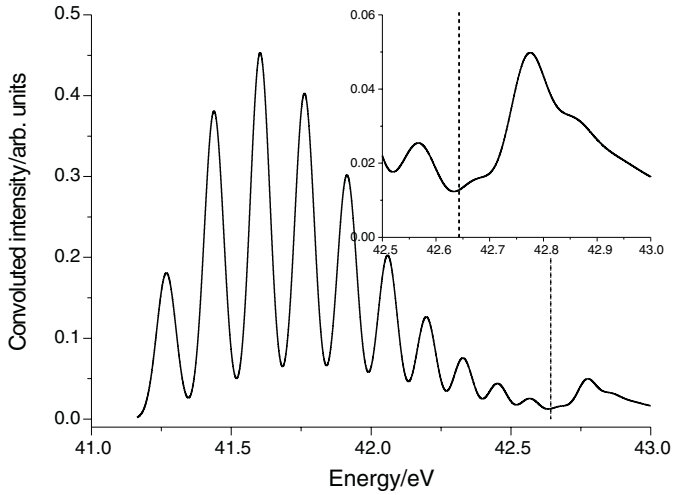

Figure 2. Calculated Franck–Condon factors for photo double ionization of ground-state neutral CO into the $X^3\Pi$ state of CO^{2+}; the vertical dotted line shows the position of the barrier maximum. The insert shows more clearly the above-barrier resonances. The above-barrier resonances clearly have greater intensity than do the highest bound levels (possibly due to accidental Franck–Condon constructive interference effects); however, this structure has not been discerned in the measured spectra.

In the present calculations we find that the calculated Franck–Condon intensities for transitions from the neutral molecule into different electronic states of the dication differ greatly in magnitude. The large numerical differences are due to the relative displacements of the potentials. We have not attempted to calculate the relative intensities for double ionization into different electronic states. In order to arrive at a simulated spectrum we therefore empirically adjusted the relative intensities of the different electronic bands as is described in detail below.

The final results of our simulations are shown in figures 3 and 4. In order to bring our calculated spectra into coincidence with the experimental measurements, adjustments had to be made to both the intensities and the frequencies.

Calculated and measured energies were brought into agreement with one another by shifting the spectra for cases (a), (b) and (d) to bring the $v = 0$ peaks for the $X^3\Pi$ state into coincidence with that of the TOF-PEPECO data. The TOF-PEPECO spectrum was chosen as the reference because the measured relative intensities within each electronic state were believed to be fairly close to Franck–Condon intensities on the basis of previous experience [36], and would therefore be most easily identified by our calculations. As the spectrum around 42 eV is severely congested this region is shown expanded in figure 4. The broad low maximum in the TPEsCO data around 48 eV arises from the reflection of the ground-state wavefunction of CO in the repulsive wall of the $c^1\Delta$ potential, and is well reproduced in our simulation.

Calculated and measured intensities were brought into broad agreement with one another by separately scaling the intensities of each vibrational progression by a single number to bring the strength of the strongest calculated and measured transition into agreement with one another. The exception to this general scheme was for the three overlapping bands shown in detail in figure 4. Here the intensity of the $X^3\Pi$ state was normalized to the $v = 0$ peak. The intensity of the $v = 0$ peak of the $a^1\Sigma^+$ spectrum at 41.4 eV was then adjusted (making

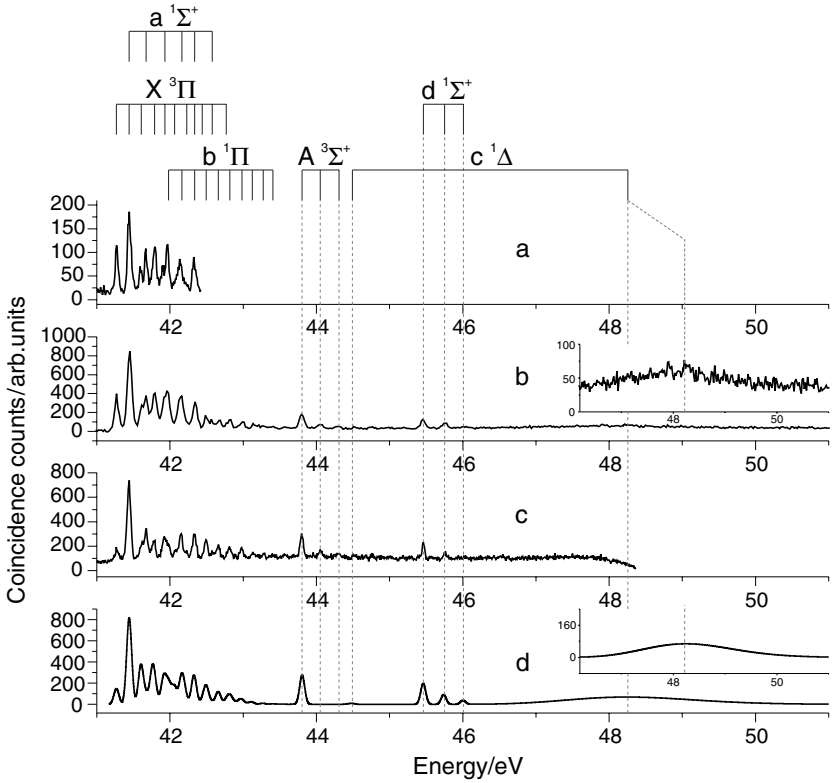

Figure 3. Showing (a) TPEsCO data from [49] shifted by −0.052 eV, (b) TPEsCO data from [48] shifted by −0.024 eV, (c) TOF-PEPECO data from [36], (d) simulated vibrational spectrum calculated in this work (see also table 8 for shifts applied to spectra (a), (b) and (d)).

allowance for the contribution of $v = 1$ of the $X^3\Pi$ state). For the $b^1\Pi$ state the band intensities were normalized to the intensity of the $v = 3$ peak (the only peak not heavily overlapped in the spectrum). The same resolved experimental peaks were used to determine how much the band origins for each separate electronic state needed to be shifted in the simulation. The final shifts used in the simulations are given in table 8. The resulting agreement between the experimental and theoretical spectra is striking, particularly in the heavily overlapped region. For example, there is a shoulder on a peak around 42 eV which is beautifully reproduced by the simulation.

The absolute double ionization energies for each band, as determined by experiment and in this work, are given in table 8. The energy zero of the calculations is $v = 0$, $J = 0$ in the neutral CO ground state. As can be seen, the different experimental measurements are in good agreement with one another. The separations and small details of spectra are well reproduced in each case, so discrepancies arise only from calibration of the absolute photon energies or electron energies. The theoretical double ionization energies calculated in the present work differ from experiment by about 1%. In order to better compare the experimental data with theory, we shifted the spectra for the other cases to align the position of the $v = 0$ peak of the $X^3\Pi$ state with that of Eland's data ((c) in figure 3).

The assignments shown above the spectra in figures 4 and 5 are those reached in the present work. We are in broad agreement with the assignments of the original experimental work, with a few exceptions which we now discuss.

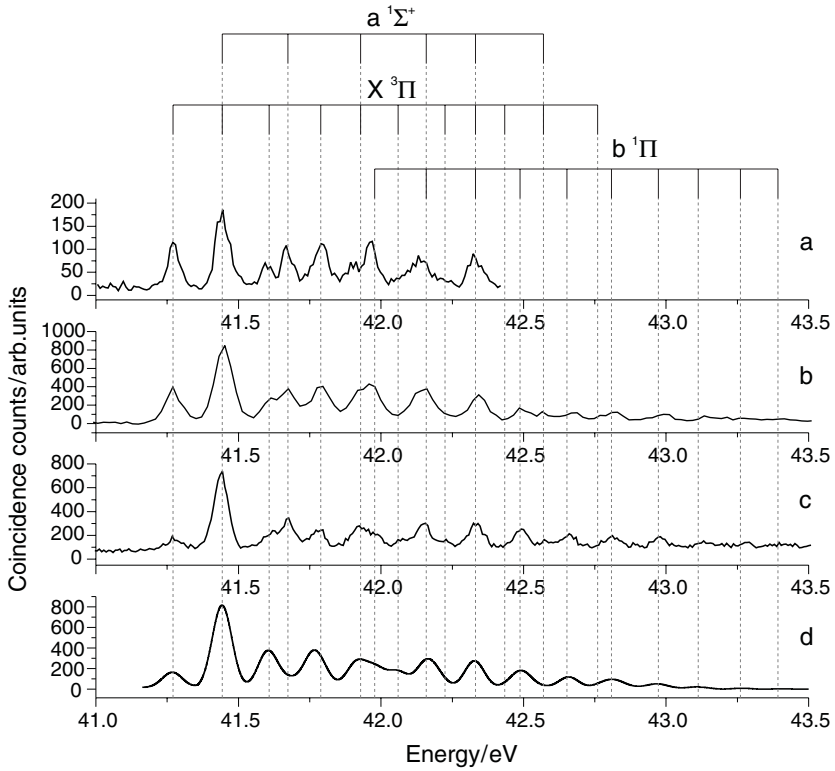

Figure 4. Segments (a), (b), (c) and (d), as in figure 3. This expanded view shows the details of the heavily overlapped spectra arising from photo double ionization to the $X^3\Pi$, $a^1\Sigma^+$ and $b^1\Pi$ states of CO^{2+}. In order to achieve best agreement with the experimental spectra, the absolute energies of the calculated bands were shifted by the amounts shown in table 8. These shifts are on average only 0.4% of the double ionization energies, amounts which are distinctly smaller than the absolute uncertainties in experiment or theory.

The energy of the $a^1\Sigma^+$ state relative to the $X^3\Pi$ ground state is accepted as given in [49], that is, the vibrational sequence begins one quantum lower than was assigned in [48]. This is confirmed both by our calculations and by the TOF-PEPECO spectrum, whose intensities are in better agreement with the Franck–Condon simulations based on the new assignment. The start of the $b^1\Pi$ sequence is easy to distinguish as a peak in the TPEsCO measurements, and as a shoulder in the TOF-PEPECO measurements, and the origin of our final simulation has been adjusted to match.

The calculations for the $d^1\Sigma^+$ state were particularly interesting. This state has a double-well (possibly triple-well) potential (see figure 1) for which the calculated (and convoluted) photoionization intensities are shown in figure 5. For our calculations of spectra the $d^1\Sigma^+$ curve was extrapolated to long bond length using an assumed C_1/R functional form (Coulomb repulsion of two charged fragments), together with an asymptotic dissociation energy of $-111.729\,50\ E_H$ (see also the discussion on linewidths in section 3.2). In order to avoid extrapolating a triple minimum potential it was necessary to omit the last calculated point on the potential curve from the extrapolation; this had no significant effect upon energy levels or Franck–Condon factors, but might affect the tunnelling predissociation linewidths substantially. As can be seen in figure 5, the photoionization

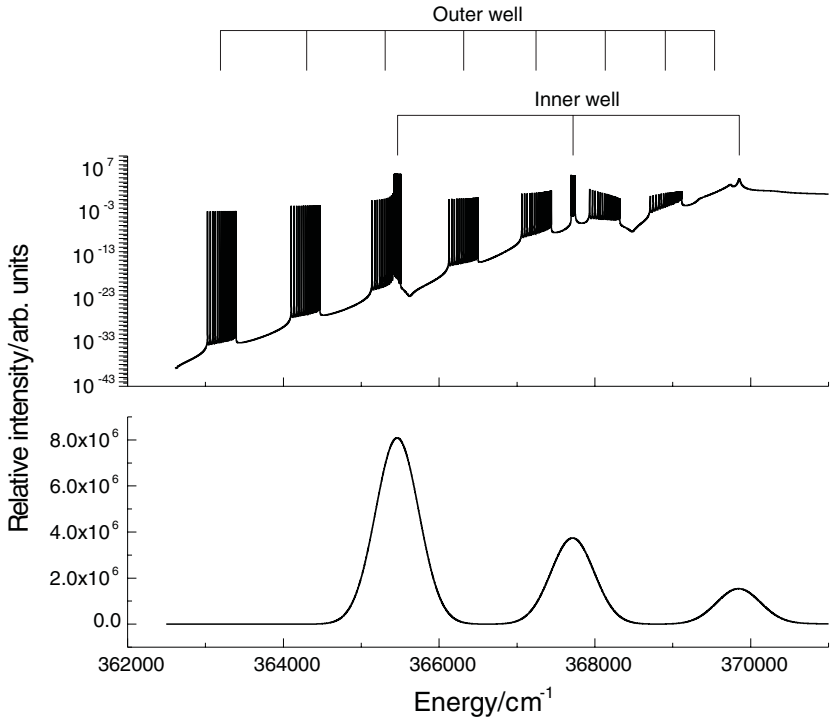

Figure 5. Calculated photoionization intensities (top) and their convolution (bottom) for excitation to the $d^1\Sigma^+$ electronic state of CO^{2+}. The double well of the $d^1\Sigma^+$ state results in two sets of vibrational levels; most of the peak intensity in the final convolution comes from the excitations to the inner well of the potential. These peaks are visible in the experimental spectrum between 45 and 46 eV.

Table 8. Band origins for vibrational progressions (of CO^{2+}) determined from photo double ionization spectra of CO, the energy zero of the calculations is $v = 0$, $J = 0$ of the neutral CO ground state. The row labelled 'Shift' is our best estimation of the energy shift required to bring the calculated vibrational sequences into coincidence with the TOF-PEPECO results.

	Band origins for vibrational progressions of the molecular dication CO^{2+}					
	$X^3\Pi$	$a^1\Sigma^+$	$b^1\Pi$	$A^3\Sigma^+$	$d^1\Sigma^+$	$c^1\Delta$
TPEsCO [48]	41.294	41.700[a]	41.814	43.573[b]	45.480	
DFKE [20]	41.300[c]	41.690	41.818	43.810	45.470	
TPEsCO [49]	41.240 ± 0.01	41.425 ± 0.01	41.757 ± 0.01			
TOF-PEPECO [36]	41.275 ± 0.03	41.438 ± 0.02	(41.780)	43.799 ± 0.03	45.461 ± 0.03	
Theory (unshifted)	41.064	41.252	41.585	43.622	45.434	43.581
Shift	0.204	0.193	0.216	0.182	0.148	0.900[d]

[a] It is suggested in [49] that the vibrational sequence begins one quantum lower than as assigned in [48]. The present analysis confirms the reassignment.
[b] It is suggested in [20] that the measured peak is not $v = 0$. If we accept the reassignment, then the value here should be 43.826 eV.
[c] The $v = 2$ level was observed, the position of $v = 0$ has been calculated by subtracting the observed TPEsCO separation [48] from the $v = 2$ energy.
[d] The shift given here is that required to bring the Franck–Condon calculated maximum at around 48 eV into coincidence with the continuum maximum in the experimental data.

cross section is a superposition of the cross-sections for transitions to the two inner wells. Noting the logarithmic intensity scale, it is clear that the three states that contribute significantly to the convolution (and are found in the experimental spectrum between 45 and 46 eV) are those in the inner well which gives rise to peaks which are narrower and more intense than those from the outer well. The peak at highest energy does, after convolution, have significant contributions from both inner-well level $v = 2$ and outer-well level $v = 7$.

No peaks were assigned to the $c^1\Delta$ state in the experimental work. For our calculations of spectra, as for the $d^1\Sigma^+$ state, no accurate extrapolation of the potential could be made to long bond length, but we assumed a C_1/R functional form (Coulomb repulsion of two charged fragments), together with an asymptotic dissociation energy of $-111.798\,07E_H$ (see also the discussion on linewidths in section 3.2). It was clear from our calculations that the extremely broad peak centred around 48 eV is due to photo fragments arising from excitation to the repulsive wall of the $c^1\Delta$ state; that is, that peak is a reflection of the $v = 0$ wavefunction of ground-state neutral CO on that repulsive wall. In order to bring our calculated position for the $c^1\Delta$ state into coincidence with the experimental position we shifted the energy of the state by 0.9 eV. With this energy shift the $v = 0$ of the $c^1\Delta$ state becomes coincident with a weak feature near 44.5 eV in the experimental spectrum; see figure 3.

We have no doubt that the reflection of the CO neutral ground-state wavefunction in the repulsive wall of the $c^1\Delta$ state is the correct explanation for the broad feature. We have brought our calculated intensity maximum into agreement with experiment by using an energy shift of 0.9 eV as this is consistent with our treatment of the other electronic states. However, the 0.9 eV shift in origin to match theory and experiment seems unreasonably large. We could also have achieved the required energy shift in the maximum in two other ways: (1) by making a small change of the relative bond lengths between the ground state of CO and the repulsive wall of the $c^1\Delta$ state or (2) by using a linear or other non-constant transition moment function; the use of a simple function in BCONT such as $\mu(R) = aR$ can readily accommodate such an energy shift. Given these considerations, it is possible, but probably unlikely, that the weak line at 44.5 eV may be due to excitation of $v = 0$ of the $c^1\Delta$ state, rather than $v = 3$ of the $A^3\Sigma^+$ state as originally assigned.

In considering the $A^3\Sigma^+$ band, it is interesting to note that our calculations find that only the $v = 0$ peak has a measurable Franck–Condon intensity; all other peaks have calculated intensities that vanish at the sensitivity of the measured spectra. It has been suggested that the relative intensities of TOF-PEPECO measurements are extremely well represented by Franck–Condon calculations with a constant transition moment function. The clear observation of a vibrational sequence for $A^3\Sigma^+$ in the TOF-PEPECO measurements contrasts starkly with our calculations using a constant transition moment function. Some of us are undertaking a study of NO^{2+} to determine more clearly if the TOF-PEPECO measurements really have intensities that can be well reproduced by Franck–Condon calculations with constant transition moment functions [47]. NO^{2+} was chosen because, unlike the present study of CO^{2+}, there are very few overlapping band systems to complicate the interpretation.

5. Conclusions

The calculations presented here show excellent general agreement with the available experimental measurements of photo double ionization spectra. The absolute accuracy of our photo double ionization energies is of order 1%, and the vibrational level separations obtained from our calculations and from experiment are in excellent agreement; the worst agreement is 0.07% (for one transition in the $b^1\Pi$ state). We believe that the potentials

reported here provide an excellent basis from which to predict high-resolution spectra that might be observed by other techniques or in astronomical measurements; such calculations will be made soon.

Acknowledgments

IMcN, GCK and JDHE are grateful to the EPSRC for support of their experimental programmes. PSK is grateful to the University of Newcastle upon Tyne for a research studentship. MH thanks the NERSC (UC Berkeley, USA) for computer time.

References

[1] See, for example, Cowley C R 1995 *An Introduction to Cosmochemistry* (Cambridge: Cambridge University Press) p 323, and references therein
[2] See, for example, Kepa R, Kocan A, Ostrowska M, Piotrowska-Domagala I, Jakubek Z and Zachwieja M 2002 *J. Mol. Spectrosc.* **214** 117
[3] Rawlings J 2003 Private communication to I R McNab
[4] See, for example, Cox S G, Critchley A D J, Kreynin P S, McNab I R, Shiell R C and Smith F E 2003 *Phys. Chem. Chem. Phys.* **5** 663, and references therein
[5] Schroder D and Schwarz H 1999 *J. Phys. Chem.* A **103** 7385
[6] Nicolaides C A 1989 *Chem. Phys. Lett.* **161** 547
[7] Radom L, Gill P M W, Wong M W and Nobes R H 1988 *Pure Appl. Chem.* **60** 183
[8] Bennett F R and McNab I R 1996 *Chem. Phys. Lett.* **251** 405
[9] Bennett F R 1995 *Chem. Phys.* **190** 53
[10] Szaflarski D M, Mullin A S, Yokoyama K, Ashfold M N R and Lineberger W C 1991 *J. Phys. Chem.* **95** 2122
[11] Bernath P F and McLeod S 2001 DiRef, a database of references associated with the spectra of diatomic molecules *J. Mol. Spectrosc.* **207** 287
[12] Wetmore R W, Le Roy R J and Boyd R K 1984 *J. Phys. Chem.* **88** 6318
[13] Larsson M, Olsson B J and Sigray P 1989 *Chem. Phys.* **139** 457
[14] Friedländer E, Kellman H, Lasereff W and Rosen B 1932 *Z. Phys.* **76** 60
[15] Penent F, Hall R I, Panajotovic R, Eland J H D, Chaplier G and Lablanquie P 1998 *Phys. Rev. Lett.* **81** 3619
[16] Bouhnik J P, Gertner I, Rosner B, Amitay Z, Heber O, Zajfman D, Sidky E Y and Ben-Itzhak I 2001 *Phys. Rev.* A **63** 032509
[17] Andersen L H, Posthumus J H, Vahtras O, Agren H, Nunez A, Scrinzi A, Natiello M and Larsson M 1993 *Phys. Rev. Lett.* **71** 1812
[18] McConkey A G, Dawber G, Avaldi L, MacDonald M A, King G C and Hall R I 1994 *J. Phys. B: At. Mol. Opt. Phys.* **27** 271
[19] Yencha A J, Juarez A M, Lee S P, King G C, Bennett F R, Kemp F and McNab I R 2004 *Chem. Phys.* **303** 179
[20] Lundqvist M, Baltzer P, Edvardsson D, Karlsson L and Wannberg B 1995 *Phys. Rev. Lett.* **75** 1058
[21] Furuhashi O, Kinugawa T, Masuda S, Yamada C and Ohtani S 2001 *Chem. Phys. Lett.* **337** 97
[22] Cossart D and Cossart-Magos C 1996 *Chem Phys. Lett.* **250** 128
[23] Cossart D and Robbe J M 1999 *Chem. Phys. Lett.* **311** 248
[24] Masters T E and Sarre P J 1990 *J. Chem. Soc. Faraday Trans.* **86** 2005
[25] Sarre P J 2002 Private communication to I R McNab
[26] Larsson M, Sundstrom G, Brostrom L and Mannervik S 1992 *J. Chem. Phys.* **97** 1750
[27] Sundstrom G, Carlson M, Larsson M and Bromstrom L 1994 *Chem. Phys. Lett.* **218** 17
[28] Pettersson L G M, Karlsson L, Keane M P, Naves de Brito A, Correia N, Larsson M, Bromstrom L, Mannervik S and Svensson S 1992 *J. Chem. Phys.* **96** 4884
[29] Pettersson L G M, Siegbahn L P E M, Bromstrom L, Mannervik S and Larsson M 1992 *Chem. Phys. Lett.* **191** 279
[30] Larsson M 2002 Private communication to I R McNab
[31] Werner H-J and Knowles P J 1985 *J. Chem. Phys.* **82** 5053
Knowles P J and Werner H-J 1985 *Chem. Phys. Lett.* **115** 259
[32] Werner H-J and Knowles J 1988 *J. Chem. Phys.* **89** 5803
Knowles P J and Werner H-J 1988 *Chem. Phys. Lett.* **145** 514
[33] Dunning T H 1989 *J. Chem. Phys.* **90** 1007

[34] Werner H-J, Knowles P J, Almlöf J, Amos R D, Deegan M J O, Elbert S T, Hampel C, Meyer W, Peterson K, Pitzer R, Stone A J and Taylor P R 2002 Molpro, a package of ab initio programs
[35] Hochlaf M, Kreynin P S, LeRoy R J, McNab I R and Robbe J-M, in preparation
[36] Eland J H D 2003 *Chem. Phys.* **294** 171
[37] Bennett F R, Critchley A D J, King G C, McNab I R and Shiell R C 2003 *Chem. Phys. Lett.* **372** 557
[38] Bennett F R, Critchley A D J, King C G, Le Roy R J and McNab I R 1999 *Mol. Phys.* **97** 35
[39] Le Roy R J 1993 *University of Waterloo Chemical Physics Research Report* CP-329R3
[40] Le Roy R J 1996 *University of Waterloo Chemical Physics Research Report* CP-555R
[41] Critchley A D J, King G C, Kreynin P S, Lopes M C A, McNab I R and Yencha A J 2001 *Chem. Phys. Lett.* **349** 79
[42] Le Roy R J and Bernstein R B 1972 *J. Chem. Phys.* **54** 5114
Pajunen P and Le Roy R J 1982 *J. Chem. Phys.* **77** 3527 (see table VI and figure 2)
[43] See, for example, Murrell J N and Bosanac S D 1989 *Introduction to the Theory of Atomic and Molecular Collisions* (Chichester: Wiley) (appendix 4)
[44] Cooley J W 1961 *Math. Comput.* **15** 363
[45] Press W H, Flannery B P, Teukolsky S A and Vettering W T (ed) 1992 *Numerical Recipes: The Art of Scientific Computing* (Cambridge: Cambridge University Press) p 383
[46] Kreynin P S 2004 *PhD Thesis* University of Newcastle upon Tyne, at press
[47] Bennett F R, Eland J H D and McNab I R, in preparation
[48] Dawber G, McConkey A G, Avaldi L, MacDonald M A, King G C and Hall R I 1994 *J. Phys. B: At. Mol. Opt. Phys.* **27** 2191
[49] Hochlaf M, Hall R I, Penent F, Kjeldsen H, Lablanquie P, Lavollée M and Eland J H D 1996 *Chem. Phys.* **207** 159